

# Magnetic-Based Minimum Input Motion Control of Paramagnetic Microparticles in Three-Dimensional Space

Islam S. M. Khalil<sup>\*b</sup>, Roel M. P. Metz<sup>\*</sup>, Bart A. Reefman<sup>\*</sup>, and Sarthak Misra<sup>\*</sup>

<sup>\*</sup>University of Twente, Enschede, The Netherlands

<sup>b</sup>German University in Cairo, New Cairo City, Egypt

**Abstract**—Magnetic drug carriers such as microrobots and paramagnetic microparticles have the potential to increase the therapeutic indices by selectively targeting the diseased tissue. These magnetic microobjects can be controlled using magnetic-based manipulation systems. In this study, we analyze a minimum input motion control to minimize the currents at each of the electromagnets of a magnetic system. This minimum input control allows us to achieve point-to-point closed-loop motion control of microparticles in the three-dimensional space, at an average speed of 198  $\mu\text{m/s}$ , and maximum root mean square position tracking error of 104  $\mu\text{m}$ . The minimum input control system is further evaluated by comparing norm-2 of its resulting current vector to the current vector of a proportional-integral (PI) control system. This comparison shows that the minimum input control achieves 11% decrease in the current input, as opposed to the PI control system. However, the PI control system achieves 43% and 285% higher average speed and positioning accuracy, respectively, as opposed to the minimum input controller. The magnetic-based minimum input control can be used to perform closed-loop control of magnetic microrobots while decreasing the current input.

## I. INTRODUCTION

Wireless motion control of magnetic microrobots [1]-[5], paramagnetic microparticles [6], [7] and magnetotactic bacteria [8]-[10] has been implemented using magnetic-based manipulation systems. These magnetic microobjects have the potential to execute tasks such as microactuation [11], micro-manipulation [12], and microassembly [13]. The execution time of these tasks can be relatively large since most of the mentioned microassembly and micromanipulation systems are not fully automated.

Martel *et al.* demonstrated a wireless magnetic-based microassembly operation of microobjects using a swarm of magnetotactic bacteria [14]. The execution time of this microassembly was approximately 15 minutes. Kummer *et al.* used the OctoMag system to puncture a blood vessel of a chorioallantoic membrane of a chicken embryo using a magnetic agent (two cubes with edge length of 800  $\mu\text{m}$ ) with permanent magnetization [15]. The execution time of this open-loop targeted drug delivery was approximately 36 seconds. Microassembly of a microobject to a microstructure is achieved using a cluster of paramagnetic microparticles

Islam S. M. Khalil, Roel M. P. Metz, Bart A. Reefman, and Sarthak Misra are affiliated with MIRA-Institute for Biomedical Technology and Technical Medicine, University of Twente.

The authors thank Leon Abelmann for his valuable feedback during preparation of this work.

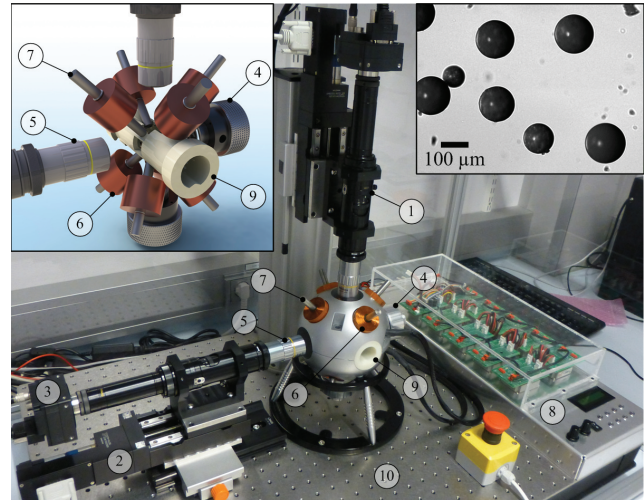


Fig. 1. Magnetic system for the wireless motion control of paramagnetic microparticles in three-dimensional space. The magnetic system allows for autofocusing using two microscopic systems ① and two linear motion stages ②. Cameras ③ with resolution and frame rate of 1024×1024 and 120 fps, respectively, are used to provide visual feedback. Illumination can be adjusted manually using 2 knobs ④. Magnification can be adjusted using the microscopic systems and objectives ⑤. The magnetic system consists of 8 electromagnetic coils ⑥ with iron cores ⑦. Current is supplied to the electromagnets using current amplifiers ⑧. A holder ⑨ is used to position a water reservoir at the center of the electromagnetic arrangement. The magnetic system is mounted on a vibration isolation table ⑩. The upper-left inset shows a rendered model of the iron-core electromagnets, reservoir holder, illumination knobs and objectives. The upper-right inset shows a microscopic image of paramagnetic microparticles in water.

by Khalil *et al.* [16]. The execution time of this open-loop microassembly operation was 18 seconds. Hu *et al.* demonstrated microassembly of polystyrene beads into different patterns using disk-shaped microrobots in approximately 17 minutes. These microrobots are optothermally steered by laser-induced bubbles [17]. Automation of the previously mentioned microassembly or drug delivery operations is not easy, since some measurements cannot be made and due to the poor understanding of the interaction forces at micro scale [18]. Therefore, the execution time of magnetic-based micromanipulation operations can be relatively large. This could limit the functionality of these systems due to the inevitable temperature increase of each of the electromagnets.

In this work, we implement a minimum input motion control system to minimize the current at each of the

electromagnets of a magnetic system (Fig. 1). This system is developed for the three-dimensional (3D) motion control of paramagnetic microparticles. First, we present a state-space model for a microparticle based on its motion under the influence of magnetic, gravitational, and drag forces. Second, we implement a linear quadratic regulator (LQR) control system to minimize the input current vector [19]. The minimum input control system is evaluated by comparing the closed-loop motion characteristics to a proportional-integral (PI) control system in the transient- and steady-states. Further, we evaluate the magnetic-based minimum input control system by comparing norm-2 of its current vector to the current vector generated using a PI control system.

The remainder of the paper is organized as follows: In Section II, we model our paramagnetic microparticle using a state-space representation, and we design a LQR control system. Experimental results of our minimum input magnetic-based control are provided in Section III, along with a comparison with a PI control system. Finally, Section IV concludes, and provides directions for future work.

## II. MODELING AND CONTROL SYSTEM DESIGN

We consider paramagnetic microparticles or a cluster of microparticles moving inside a fluid under the influence of the external magnetic fields. First, we derive a state-space representation of a microparticle. Second, we use this state-space representation in the realization of a minimum input closed-loop control law that minimizes the current vector at each of the electromagnets of our magnetic system.

### A. Modeling of Paramagnetic Microparticles

Under the influence of magnetic forces, drag forces and buoyancy forces, motion of a microparticle in a fluid is given by

$$\mathbf{F}(\mathbf{P}) - \mathbf{F}_d(\dot{\mathbf{P}}) - F_b \hat{\mathbf{n}} = M\ddot{\mathbf{P}}, \quad (1)$$

where  $\mathbf{F}(\mathbf{P}) \in \mathbb{R}^{3 \times 1}$ ,  $\mathbf{F}_d(\dot{\mathbf{P}}) \in \mathbb{R}^{3 \times 1}$  and  $F_b \in \mathbb{R}^{1 \times 1}$  are the magnetic force, drag force, and buoyancy force at a position ( $\mathbf{P} \in \mathbb{R}^{3 \times 1}$ ), respectively. Further,  $M$  is the mass of the microparticle. The inertial term in (1) can be ignored at a low Reynolds number regime, and  $\hat{\mathbf{n}} \in \mathbb{R}^{3 \times 1}$  is a unit vector of the buoyancy force. In (1), the magnetic force is given by

$$\mathbf{F}(\mathbf{P}) = \nabla(\mathbf{m}(\mathbf{P}) \cdot \mathbf{B}(\mathbf{P})). \quad (2)$$

In (2),  $\mathbf{m}(\mathbf{P}) \in \mathbb{R}^{3 \times 1}$  and  $\mathbf{B}(\mathbf{P}) \in \mathbb{R}^{3 \times 1}$  are the permanent or induced magnetic dipole moment of the microparticle and the induced magnetic field at point ( $\mathbf{P} \in \mathbb{R}^{3 \times 1}$ ), respectively [20], [21]. The drag force is given by

$$\mathbf{F}_d(\dot{\mathbf{P}}) = 6\pi\eta r_p \dot{\mathbf{P}}, \quad (3)$$

where  $\eta$  and  $r_p$  are the fluid dynamic viscosity and the radius of the microparticle, respectively. Finally, the net buoyancy force is given by

$$F_b = V(\rho_p - \rho_f)g. \quad (4)$$

In (4),  $V$  and  $\rho_p$  are the volume and density of the microparticle, respectively. Further,  $\rho_f$  and  $g$  are the density of the

fluid and the acceleration due to gravity, respectively. We represent (1) using the following state-space representation:

$$\begin{aligned} \dot{\mathbf{x}}_k &= \mathbf{x}_{k+1}, \\ \dot{\mathbf{x}}_{k+1} &= \mathbf{M}^{-1}(\mathbf{F}_j(\mathbf{P}) - 6\pi\eta r_p \mathbf{x}_{k+1}) - F_{b_j}, \end{aligned} \quad (5)$$

where  $\mathbf{x}_k$  is the  $k$ th state of a microparticle (for  $k = 1, 2, 3$ ). Further,  $F_j(\mathbf{P})$  and  $F_{b_j}$  are the  $j$ th component of the magnetic and buoyancy forces, respectively (for  $j = x, y, z$ ). In (5),  $\mathbf{x}_k$  and  $\dot{\mathbf{x}}_k$  represent the position and velocity of the microparticle along the  $j$ -axis, respectively (for  $j = x, y, z$ ).

We represent (5) and (6) using the following standard state-space representation:

$$\dot{\mathbf{x}} = \mathbf{A}\mathbf{x} + \mathbf{B}\mathbf{u}. \quad (7)$$

In (7),  $\mathbf{A} \in \mathbb{R}^{6 \times 6}$  and  $\mathbf{B} \in \mathbb{R}^{6 \times 1}$  are the system matrix and the distribution vector of the magnetic force input, respectively. Further,  $\mathbf{x} \in \mathbb{R}^{6 \times 1}$  and  $\mathbf{u} \in \mathbb{R}^{6 \times 1}$  are the state and input vectors, respectively. Our goal is to regularize the states of a microparticle or a microrobot using a set of control inputs that minimizes the current at each of the electromagnets of the magnetic system.

### B. Minimum Input Control System Design

In order to minimize the current at each of the electromagnets we devise the following performance measure ( $J$ ):

$$J = \int_{t_0}^{t_f} \frac{1}{2} (\mathbf{u}^T \mathbf{R} \mathbf{u}) dt, \quad (8)$$

where  $\mathbf{R} \in \mathbb{R}^{6 \times 6}$  is a symmetric positive-definite matrix. Further,  $t_0$  and  $t_f$  are the initial and final time of a 3D point-to-point closed-loop motion control of the microparticle, respectively. Using (6), the input vector ( $\mathbf{u}$ ) is given by

$$\mathbf{u} = \begin{bmatrix} 0 & F_x(\mathbf{P}) & 0 & F_y(\mathbf{P}) & 0 & F_z(\mathbf{P}) - F_{b_z} \end{bmatrix}^T. \quad (9)$$

The magnetic force components in (9) can be explicitly represented using the current ( $I_i$ ) at the  $i$ th electromagnet of the magnetic system (for  $i = 1, \dots, n$ ). The magnetic force components are related to the currents at each of the electromagnets using

$$F_j(\mathbf{P}) = \beta \mathbf{I}^T \left( \frac{\partial(\tilde{\mathbf{B}}^T(\mathbf{P})\tilde{\mathbf{B}}(\mathbf{P}))}{\partial j} \right) \mathbf{I} \text{ for } j = x, y, z, \quad (10)$$

where  $\beta$  is a constant and is given by

$$\beta \triangleq \frac{4}{3} \frac{1}{\mu} \pi r_p^3 \chi_m. \quad (11)$$

In (11),  $\mu$  and  $\chi_m$  are the permeability coefficient and magnetic susceptibility constant. Further,  $\tilde{\mathbf{B}}(\mathbf{P}) \in \mathbb{R}^{3 \times n}$  is a matrix that maps the current vector ( $\mathbf{I} \in \mathbb{R}^{n \times 1}$ ) onto magnetic field ( $\mathbf{B}(\mathbf{P}) \in \mathbb{R}^{3 \times 1}$ ) [15]

$$\mathbf{B}(\mathbf{P}) = \sum_{i=1}^n \tilde{\mathbf{B}}_i(\mathbf{P}) I_i = \tilde{\mathbf{B}}(\mathbf{P}) \mathbf{I}, \quad (12)$$

where  $n$  is the number of electromagnets within our magnetic system. Further,  $\tilde{\mathbf{B}}_i(\mathbf{P})$  and  $I_i$  are the magnetic field-current

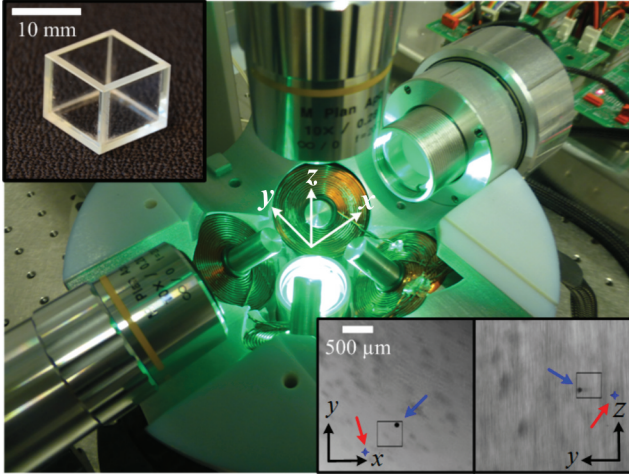


Fig. 2. Magnetic system for the closed-loop motion control of paramagnetic microparticles (PLAParticles-M-redF-plain from Micromod Partikeltechnologie GmbH, Rostock-Warnemuende, Germany) in three-dimensional (3D) space. The magnetic system consists of 8 iron-core electromagnets that surrounds a water reservoir, shown at the upper-left inset. The workspace of the magnetic system is  $10 \times 10 \times 10 \text{ mm}^3$ . Our magnetic system provides autofocusing of the microparticles using two microscopic vision systems mounted on two linear motion stages (not shown). The magnetic system consists of upper and lower orthogonal sets of electromagnets. In the lower set, the electromagnets have 45 degrees orientation with respect to each other and with respect to the horizontal plane. In the upper set (not shown), electromagnets have 45 degrees and 90 degrees orientation with respect to the horizontal plane and the lower set, respectively. The bottom-right inset shows a microparticle, with an average diameter of  $100 \mu\text{m}$ , moving towards a reference position in 3D space under the influence of the controlled magnetic fields generated using the minimum input control (13). The black box is assigned using our feature tracking software, whereas the blue and red arrows indicate the microparticle and the reference position, respectively.

map and current at the  $i$ th electromagnet, respectively. The control input (9) along with the magnetic force-current map (10) indicates that, minimizing the input ( $\mathbf{u}$ ) minimizes the current vector ( $\mathbf{I}$ ). The minimum input control law that minimizes the performance measure (8) is given by

$$\mathbf{u} = -\mathbf{R}^{-1}\mathbf{B}^T\mathbf{K}\mathbf{x}, \quad (13)$$

where  $\mathbf{K} \in \mathbb{R}^{6 \times 6}$  is a symmetric positive-definite matrix that satisfies the following Riccati differential equation [19]:

$$\dot{\mathbf{K}} - \mathbf{KBR}^{-1}\mathbf{B}^T\mathbf{K} + \mathbf{KA} + \mathbf{A}^T\mathbf{K} = 0. \quad (14)$$

Control law (13) regulates the states of the microparticles to a given reference position. This minimum input control law is used in the realization of point-to-point control in 3D space.

### III. EXPERIMENTAL RESULTS

Closed-loop motion control results are done using a magnetic system with paramagnetic microparticles. First, we implement the minimum input controller using (13) and (14). Second, we implement a PI control system. The closed-loop motion control characteristics and the sum of norm-2 of the generated current vectors of each control system are used to evaluate our magnetic-based minimum input control strategy.

TABLE I

SPECIFICATIONS OF THE MAGNETIC SYSTEM AND THE CONTROLLER GAINS. MAXIMUM FIELDS AND GRADIENTS ARE PROVIDED. THE GAINS ARE SELECTED SUCH THAT THE MATRIX ( $\mathbf{K}$ ) SATISFIES THE RICCATI DIFFERENTIAL EQUATION AND BASED ON THE DIAGONAL MATRIX ( $\mathbf{R}$ ).

FURTHER,  $r_l$  DENOTES THE ENTRIES OF THE MATRIX ( $\mathbf{R}$ ) FOR ( $l = 1, \dots, 6$ ). THE MATRICES ( $\mathbf{K}_p$  AND  $\mathbf{K}_i$ ) ARE POSITIVE DEFINITE.

FURTHER,  $k_{p1,2,3}$  AND  $k_{i1,2,3}$  REPRESENT THE ENTRIES OF THE MATRICES ( $\mathbf{K}_p$  AND  $\mathbf{K}_i$ ), RESPECTIVELY.

Parameter	Value	Parameter	Value
$\max I_i$ [A]	2.0	Workspace [ $\text{mm}^3$ ]	$10 \times 10 \times 10$
$ \mathbf{B}(\mathbf{P}) $ [mT]	85	$\nabla \mathbf{B}(\mathbf{P}) $ [ $\text{T}\cdot\text{m}^{-1}$ ]	1.62
$B_x(\mathbf{P})$ [mT]	39.4	$\frac{\partial B(\mathbf{P})}{\partial x}$ [ $\text{T}\cdot\text{m}^{-1}$ ]	0.49
$B_y(\mathbf{P})$ [mT]	38.2	$\frac{\partial B(\mathbf{P})}{\partial y}$ [ $\text{T}\cdot\text{m}^{-1}$ ]	0.37
$B_z(\mathbf{P})$ [mT]	64.5	$\frac{\partial B(\mathbf{P})}{\partial z}$ [ $\text{T}\cdot\text{m}^{-1}$ ]	1.52
$n$	8	Frame per second	120
$r_p$ [ $\mu\text{m}$ ]	50	$\eta$ [mPa.s]	1.0
$k_{p1,2,3}$ [ $\text{s}^{-2}$ ]	0.14	$k_{i1,2,3}$ [s]	0.08
$r_{1,2,3,4}$	2	$M$ [kg]	$7.33 \times 10^{-10}$
$r_{5,6}$	0.8	$\mu_0$ [ $\text{T}\cdot\text{m}\cdot\text{A}^{-1}$ ]	$4\pi \times 10^{-7}$

#### A. Magnetic System

Our magnetic system consists of two orthogonal sets of iron-core electromagnets. Each set is mounted inside a hemispherical structure that holds a water reservoir at its center (Fig. 1). The lower set consists of 4 orthogonal electromagnets. Each of these electromagnets has an orientation of 45 degrees with the horizontal plane, as shown in Fig. 2. The upper set also consists of 4 orthogonal electromagnets. Each electromagnet has an orientation of 45 degrees with respect to the horizontal plane. The lower and upper sets are mounted orthogonally with respect to each other. The magnetic system is equipped with two microscopic systems (Optem<sup>®</sup> Zoom 125C, QIOPTIQ, Luxembourg) and two linear motion stages (M-404.2DG Precision Translation Stage, Karlsruhe, Germany) to achieve autofocusing of microparticles. This system is capable of generating maximum magnetic fields and field gradients of 85 mT and 1.62 T/m, respectively. We utilize microparticles (PLAParticles-M-redF-plain from Micromod Partikeltechnologie GmbH, Rostock-Warnemuende, Germany) with average diameter of  $100 \mu\text{m}$  throughout our experimental work. Table I includes the specifications of our magnetic system.

#### B. Minimum Input Motion Control

The minimum input motion control law (13) depends on the nominal values of the parameters of our magnetic system. First, the matrices ( $\mathbf{A}$  and  $\mathbf{B}$ ) are calculated based on (5) and (6). Second, the gain matrix ( $\mathbf{K}$ ) is determined using (14). We assume that the matrices ( $\mathbf{A}$  and  $\mathbf{B}$ ) have constant parameters. Therefore,  $\mathbf{K} \in \mathbb{R}^{6 \times 6}$  is calculated off-line and used in the realization of the control law (13). This is a valid assumption since the entries of the matrices ( $\mathbf{A}$  and  $\mathbf{B}$ ) are constant. The entries of the diagonal positive-definite matrix ( $\mathbf{R} \in \mathbb{R}^{6 \times 6}$ ) are selected to be 2, 2, 2, 2, 0.8, and

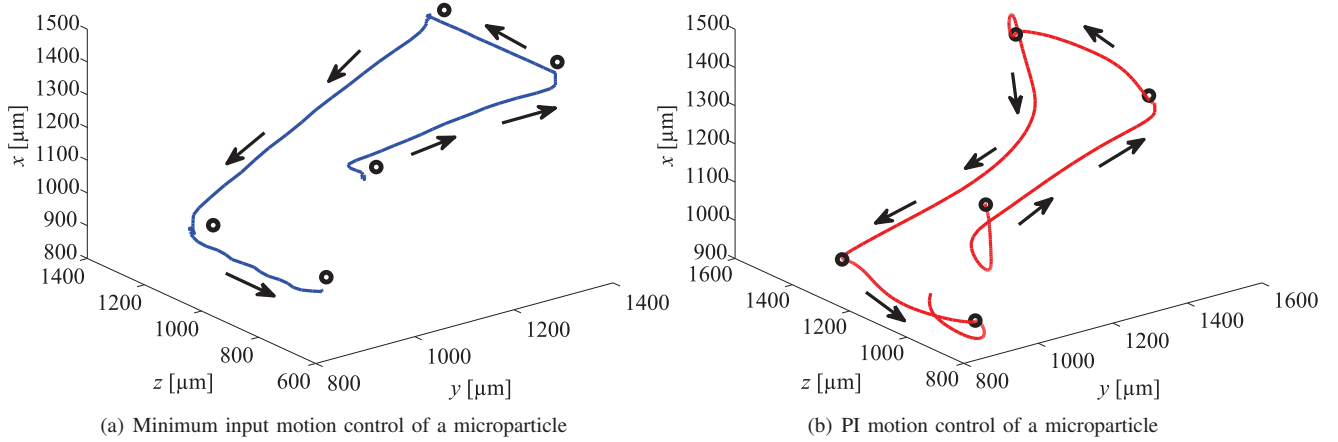


Fig. 3. Motion control of a paramagnetic microparticle in three-dimensional (3D) space under the influence of the controlled magnetic fields. The microparticle follows a rectangular trajectory in the 3D space by following 4 reference positions (black circles). Motion of the microparticle is controlled using the minimum input motion control law (13) and the proportional-integral (PI) control law (15). First, the minimum input motion control law is applied, and then the PI control law is used to control the same microparticle. The black arrows indicate the direction of the controlled microparticle. (a) Minimum input motion control: In this representative motion control result, the minimum input control system positions the microparticle at an average speed of  $198 \mu\text{m/s}$ , and maximum root mean square (RMS) position tracking error of  $104 \mu\text{m}$ . The entries of the diagonal matrix ( $\mathbf{R} \in \mathbb{R}^{6 \times 6}$ ) are 2, 2, 2, 0.8, and 0.8. (b) PI motion control: In this representative motion control result, the PI control system positions the microparticle at an average speed of  $283 \mu\text{m/s}$ , and maximum RMS position tracking error of  $7 \mu\text{m}$ . The entries of the proportional gain diagonal matrix ( $\mathbf{K}_p \in \mathbb{R}^{3 \times 3}$ ) are 0.14, 0.14 and 0.14, whereas the entries of the integral gain diagonal matrix ( $\mathbf{K}_i \in \mathbb{R}^{3 \times 3}$ ) are 0.08, 0.08 and 0.08. Please refer to the attached video that demonstrates the results of our magnetic-based minimum input and PI motion control experiments.

0.8. Fig. 3(a) shows a representative minimum input motion control result of a paramagnetic microparticle. In this experiment, the microparticle follows a rectangular trajectory in 3D space by tracking 4 reference positions (black circles). We observe that the microparticle tracks the reference positions at speeds of  $90 \mu\text{m/s}$ ,  $125 \mu\text{m/s}$ , and  $125 \mu\text{m/s}$  along  $x$ -,  $y$ - and  $z$ -axis, respectively. Further, the minimum input motion control system achieves position tracking error of  $25 \mu\text{m}$ ,  $14 \mu\text{m}$ , and  $100 \mu\text{m}$  along  $x$ -,  $y$ - and  $z$ -axis, respectively. Figs. 4(a), (b), and (c) show the motion components along  $x$ -,  $y$ -, and  $z$ -axis of the controlled microparticle under the influence of the minimum input motion control. We repeated this motion control experiment 5 times, the average speed and the maximum root mean square (RMS) position tracking errors of the controlled microparticle are calculated to be  $198 \mu\text{m/s}$  and  $104 \mu\text{m}$ , respectively. Please refer to the attached video that demonstrates the results of our magnetic-based minimum input motion control experiments.

Characteristics of the minimum input motion control system are compared to a PI control system. This comparison is achieved by switching the minimum input control to PI control. The motion components of the microparticle are represented using the blue and red solid lines for the minimum input and PI control, respectively. In the representative motion control result, shown in Fig. 3(b) and Fig. 4, the PI control system is initialized at time instant (Time=335 s), and a similar motion control trail to the minimum input motion control is initiated at time instant (Time=395 s).

### C. Proportional-Integral Control

In order to show that the minimum input magnetic-based control system indeed decreases the current at each of the

electromagnets, we devise a PI control system and compare its motion control characteristics to the minimum input control system. In this case, the control input is given by

$$\mathbf{u} = \mathbf{K}_p \mathbf{e} + \mathbf{K}_i \int_{t_0}^{t_f} \mathbf{e} dt, \quad (15)$$

where  $\mathbf{K}_p \in \mathbb{R}^{3 \times 3}$  and  $\mathbf{K}_i \in \mathbb{R}^{3 \times 3}$  are the proportional and integral gain matrices, respectively. Further,  $\mathbf{e} \in \mathbb{R}^{3 \times 1}$  is the position tracking error and is given by

$$\mathbf{e} = \mathbf{P} - \mathbf{P}_{\text{ref}}. \quad (16)$$

In (16),  $\mathbf{P}_{\text{ref}} \in \mathbb{R}^{3 \times 1}$  is a fixed reference position. Fig. 3(b) shows a representative motion control of a microparticle in 3D space using the PI control law (15). In this experiment, the microparticle follows the same 4 reference positions used for the minimum input control trials. The entries of the diagonal matrices ( $\mathbf{K}_p$  and  $\mathbf{K}_i$ ) are selected to be 0.14 and 0.08, respectively. As shown in Fig. 4, the PI control system is initialized and applied. We observe that the microparticle tracks the reference positions at speeds of  $125 \mu\text{m/s}$ ,  $250 \mu\text{m/s}$ , and  $156 \mu\text{m/s}$  along  $x$ -,  $y$ - and  $z$ -axis, respectively. Further, the PI motion control system achieves position tracking error of  $4 \mu\text{m}$ ,  $3 \mu\text{m}$ , and  $5 \mu\text{m}$  along  $x$ -,  $y$ - and  $z$ -axis, respectively. We repeated this motion control experiment 5 times, the average speed and the maximum RMS position tracking error of the controlled microparticle are calculated to be  $283 \mu\text{m/s}$  and  $27 \mu\text{m}$ , respectively. Please refer to the attached video that demonstrates the results of our magnetic-based PI motion control experiments.

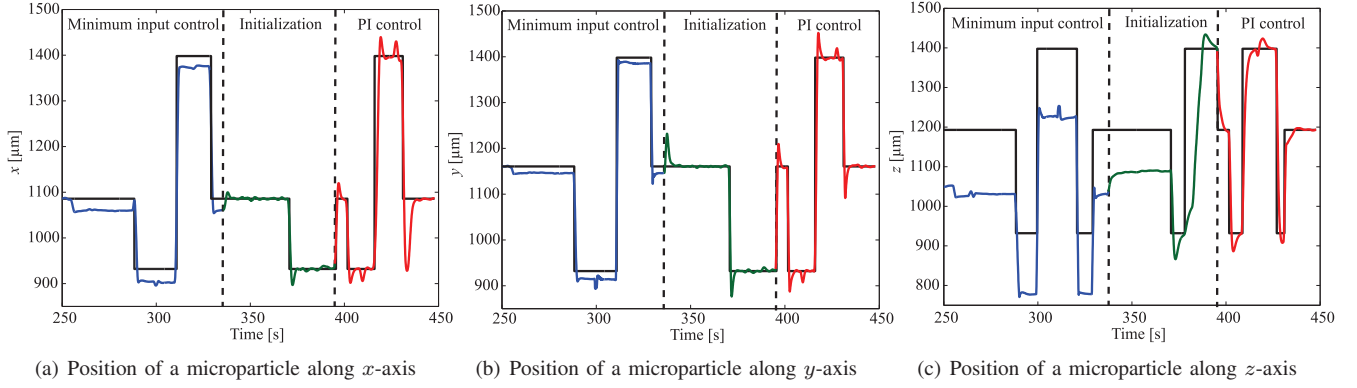


Fig. 4. Motion control of a paramagnetic microparticle in three-dimensional space under the influence of the controlled magnetic fields. The microparticle follows a square trajectory using the minimum input motion control (13) and the proportional-integral (PI) control (15). The minimum input motion control is applied until the time instant (Time=335 s). At this instant, the control system initializes and switches to PI control system at the time instant (Time=395 s). The black solid lines represent the components of the reference positions, whereas the blue and red solid lines represent the motion components of the microparticle under the influence of the minimum input and PI control systems, respectively. The green lines represent the motion components of the microparticle during the initialization of the PI control system. The entries of the diagonal matrix ( $\mathbf{R} \in \mathbb{R}^{6 \times 6}$ ) are 2, 2, 2, 2, 0.8, and 0.8, respectively. The entries of the diagonal matrix ( $\mathbf{K}_p \in \mathbb{R}^{3 \times 3}$ ) are 0.14, 0.14 and 0.14, whereas the entries of the diagonal matrix ( $\mathbf{K}_i \in \mathbb{R}^{3 \times 3}$ ) are 0.08, 0.08 and 0.08. (a) Motion of the microparticle along  $x$ -axis: The average velocity component along  $x$ -axis is  $90 \mu\text{m/s}$ , and the maximum position tracking error is  $25 \mu\text{m}$  using the minimum input control system. The PI control system positions the same microparticle at a speed and maximum position tracking error of  $125 \mu\text{m/s}$ , and  $4 \mu\text{m}$ , respectively. (b) Motion of the microparticle along  $y$ -axis: The average velocity component along  $y$ -axis is  $125 \mu\text{m/s}$ , and the maximum position tracking error is  $14 \mu\text{m}$  using the minimum input control system. The PI control system positions the same microparticle at a speed and maximum position tracking error of  $250 \mu\text{m/s}$ , and  $3 \mu\text{m}$ , respectively. (c) Motion of the microparticle along  $z$ -axis: The average velocity component along  $z$ -axis is  $125 \mu\text{m/s}$ , and the maximum position tracking error is  $100 \mu\text{m}$  using the minimum input control system. The PI control system positions the same microparticle at a speed and maximum position tracking error of  $156 \mu\text{m/s}$ , and  $5 \mu\text{m}$ , respectively. Please refer to the attached video that demonstrates the results of our magnetic-based minimum input and PI motion control experiments.

#### D. Minimum Input Versus Proportional-Integral Control

The generated current vectors using the magnetic-based minimum input and PI control systems are recorded for each motion control trial. We calculate norm-2 of the generated current vectors using

$$\|\mathbf{I}\|_2 = \left( \sum_{i=1}^n I_i^2 \right)^{1/2}; \quad \mathbf{I} = [I_1 \quad \dots \quad I_8]^T. \quad (17)$$

Fig. 5 shows the calculated norm-2 of the generated current vectors using the minimum input and PI control systems. The blue and red solid lines represent norm-2 of the generated current vectors using the aforementioned control systems during similar control trials. The green line represents norm-2 of the current vector during the initialization of the PI control system. The control results provided in Fig. 3 and Fig. 4 are obtained using the current inputs shown in Fig. 5. We observe that the minimum input control system achieves 11% decrease in the generated current input, as opposed to the PI control system. This decrease indicates that our minimum input control system indeed reduces the current at each of the electromagnets. However, the PI control system provides higher average speed and positioning accuracy than the minimum input control system. Table II summarizes the comparison between the minimum input and PI control systems. The PI control achieves 43% and 285% higher average speed and positioning accuracy than the minimum input control. The difference in the positioning accuracy is due to the position tracking error along  $z$ -axis, as shown in Fig. 4(c). We attribute this difference to the nature of the minimum input control since it generates current vector

that minimizes the performance measure (8). However, this current vector does not allow the microparticles to overcome the vertical components of the drag and buoyancy forces. Excluding the vertical component of the average velocity and position tracking error from our calculations shows that the PI control system achieves 47% and 81% higher average speed and positioning accuracy, respectively, as opposed to the minimum input control system.

The control characteristics of the minimum input control system can be improved by incorporating the sum squared of the position tracking error in the performance measure (8). This would allow us to determine a control system that reduces the input current vector and increases the positioning accuracy of the controlled microparticles.

#### IV. CONCLUSIONS AND FUTURE WORK

We investigate a magnetic-based minimum input control system to position paramagnetic microparticles in 3D space. The minimum input control system achieves point-to-point motion control, while minimizing the current at each of the electromagnets of a magnetic system. The closed-loop control characteristics of the magnetic-based minimum input control are compared to the characteristics of a PI controller. We observe that the PI control achieves 43% and 285% higher average speed and positioning accuracy, as opposed to the minimum input control system. However, the minimum input control system decreases the sum of norm-2 of the current input vector by 11%, as opposed to the PI control system. This decrease could allow us to reduce the generated heat at each of the electromagnets, and increase the availability of magnetic systems for tasks, such as micromanipulation,

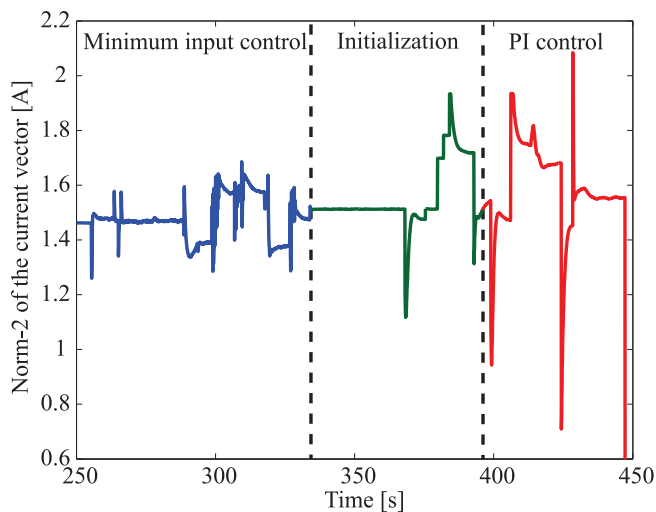


Fig. 5. Norm-2 of the generated current vectors using the minimum input control law (13) and the proportional-integral (PI) control law (15). The blue and red solid lines represent norm-2 of the current vector ( $\mathbf{I} \in \mathbb{R}^{8 \times 1}$ ) generated using the minimum input and the PI control systems, respectively. The green line represents norm-2 of the current vector during the initialization of the PI control system. Currents at each of the electromagnets of our magnetic system are recorded during a representative motion control trial. In this trial the minimum input motion control is switched to PI control at the time instant (Time=395 s). The resulting norm-2 of the current vector of the minimum input control system is 11% less than norm-2 of the generated current vector of the PI control system. The minimum input and PI control systems allow the microparticle to follow a rectangular trajectory by tracking four reference positions.

microassembly, microactuation and targeted drug delivery.

As part of future work, our magnetic system will be integrated with a clinical imaging modality [8]. In addition, a microfluidic channel will be incorporated with our magnetic system to investigate the control characteristics in the presence of time-varying flow rates. The positioning accuracy of the minimum input control system will be improved by incorporating the sum of squared of the position tracking error to the performance measure (8).

## REFERENCES

- [1] J. J. Abbott, Z. Nagy, F. Beyeler, and B. J. Nelson, "Robotics in the small, part I: microbotics," *IEEE Robotics and Automation Magazine*, vol. 14, no. 2, pp. 92-103, June 2007.
- [2] C. Pawashe, S. Floyd, E. Diller, and M. Sitti, "Two-dimensional autonomous microparticle manipulation strategies for magnetic microrobots in fluidic environments," *IEEE Transactions on Robotics*, vol. 28, no. 2, pp. 467-477, April 2012.
- [3] L. Dong and B. J. Nelson, "Tutorial-Robotics in the small part II: nanorobotics," *IEEE Robotics and Automation Magazine*, vol. 14, no. 3, pp. 111-121, September 2007.
- [4] J. J. Abbott, O. Ergeneman, M. P. Kummer, A. M. Hirt, and B. J. Nelson, "Modeling magnetic torque and force for controlled manipulation of soft-magnetic bodies," *IEEE Transactions on Robotics and Automation*, vol. 23, no. 6, pp. 1247-1252, December 2007.
- [5] I. S. M. Khalil, J. D. Keuning, L. Abelmann, and S. Misra, "Wireless magnetic-based control of paramagnetic microparticles," in *Proceedings of the IEEE RAS/EMBS International Conference on Biomedical Robotics and Biomechanics (BioRob)*, pp. 460-466, Rome, Italy, June 2012.
- [6] J.-B. Mathieu and S. Martel, "Steering of aggregating magnetic microparticles using propulsion gradients coils in an MRI scanner," *Magnetic Resonance in Medicine*, vol. 63, no. 5, pp. 1336-1345, May 2010.

TABLE II

CLOSED-LOOP CONTROL CHARACTERISTICS OF CONTROLLED PARAMAGNETIC MICROPARTICLES USING THE MINIMUM INPUT CONTROL LAW (13) AND THE PROPORTIONAL-INTEGRAL (PI) CONTROL LAW (15). THE AVERAGE VELOCITIES AND THE MAXIMUM POSITION TRACKING ERRORS ARE CALCULATED FROM 5 MOTION CONTROL TRIALS FOR EACH CONTROL SYSTEM. THE SUM OF NORM-2 OF THE CURRENT VECTOR ( $\sum \|\mathbf{I}\|_2$ ) IS USED TO EVALUATE THE PERFORMANCE OF THE MINIMUM INPUT AND PI CONTROL SYSTEMS.

Characteristics	Minimum input	PI
Average speed [ $\mu\text{m/s}$ ]	$198 \pm 20$	$283 \pm 25$
Maximum tracking error [ $\mu\text{m}$ ]	104	27
$\sum \ \mathbf{I}\ _2$ [A]	885.7	994.8

- [7] I. S. M. Khalil, R. M. P. Metz, L. Abelmann, and S. Misra, "Interaction force estimation during manipulation of microparticles," in *Proceedings of the IEEE International Conference of Robotics and Systems (IROS)*, pp. 950-956, Vilamoura, Portugal, October 2012.
- [8] S. Martel, O. Felfoul, J.-B. Mathieu, A. Chanu, S. Tamaz, M. Mohammadi, M. Mankiewicz, and N. Tabatabaei, "MRI-based medical nanorobotic platform for the control of magnetic nanoparticles and flagellated bacteria for target interventions in human capillaries," *The International Journal of Robotics Research*, vol. 28, no. 9, pp. 1169-1182, September 2009.
- [9] I. S. M. Khalil, M. P. Pichel, L. Zondervan, L. Abelmann, and S. Misra, "Characterization and control of biological microrobots," in *Proceedings of the 13th International Symposium on Experimental Robotics-Springer Tracts in Advanced Robotics*, Springer Tracts in Advanced Robotics (STAR), vol. 88, pp. 617-631, 2013.
- [10] I. S. M. Khalil, M. P. Pichel, L. Abelmann, and S. Misra, "Closed-loop control of magnetotactic bacteria," *The International Journal of Robotics Research*, vol. 32, no. 6, pp. 637-649, May 2013.
- [11] S. Martel, "Controlled bacterial micro-actuation," in *Proceedings of the International Conference on Microtechnologies in Medicine and Biology*, pp. 89-92, Okinawa, Japan, May 2006.
- [12] C. Pawashe, S. Floyd, E. Diller, and M. Sitti, "Two-dimensional autonomous microparticle manipulation strategies for magnetic microrobots in fluidic environments," *IEEE Transactions on Robotics*, vol. 28, no. 2, pp. 467-477, April 2012.
- [13] S. Martel and M. Mohammadi, "Towards mass-scale micro-assembly systems using magnetotactic bacteria," *International Manufacturing Science and Engineering Conference (ASME)*, vol. 2, no. 6, pp. 487-492, Oregon, USA, June 2011.
- [14] S. Martel and M. Mohammadi, "Using a swarm of self-propelled natural microrobots in the form of flagellated bacteria to perform complex micro-assembly tasks," in *Proceedings of the IEEE International Conference on Robotics and Automation (ICRA)*, pp. 500-505, Alaska, USA, May 2010.
- [15] M. P. Kummer, J. J. Abbott, B. E. Kartochovil, R. Borer, A. Sengul, and B. J. Nelson, "OctoMag: an electromagnetic system for 5-DOF wireless micromanipulation," *IEEE Transactions on Robotics*, vol. 26, no. 6, pp. 1006-1017, December 2010.
- [16] I. S. M. Khalil, F. van den Brink, O. S. Sukas, and S. Misra, "Microassembly using a cluster of paramagnetic microparticles," in *Proceedings of the IEEE International Conference on Robotics and Automation (ICRA)*, pp. 5507-5512, Karlsruhe, Germany, May 2013.
- [17] W. Hu, K. S. Ishii, Q. Fan, and A. T. Ohta, "Hydrogel microrobots actuated by optically generated vapour bubbles," *Lap on a Chip*, vol. 12, no. 19, pp. 3821-3826, 2012.
- [18] M. Savia and H. N. Koivo, "Contact micromanipulation—survey of strategies," *IEEE/ASME Transactions on Mechatronics*, vol. 14, no. 4, pp. 504-514, August 2009.
- [19] D. E. Kirk, "Optimal control theory: an introduction," *Dover Publications, Inc*, Mineola, New York, 2004.
- [20] T. H. Boyer, "The force on a magnetic dipole," *American Journal of Physics*, vol. 56, no. 8, pp. 688-692, August 1988.
- [21] S. S. Shevkoplyas, A. C. Siegel, R. M. Westervelt, M. G. Prentiss, and G. M. Whitesides, "The force acting on a superparamagnetic bead due to an applied magnetic field," *Lab on a Chip*, vol. 7, no. 6, pp. 1294-1302, July 2007.